Multiband and nonlinear hopping corrections to the three-dimensional Bose-Fermi-Hubbard model

Alexander Mering and Michael Fleischhauer
Fachbereich Physik and Research Center for Optics and Material Sciences, Technische Universität Kaiserslautern, D-67663 Kaiserslautern, Germany

(Received 10 September 2010; revised manuscript received 1 April 2011; published 27 June 2011)

Recent experiments revealed the importance of higher-band effects for the Mott-insulator(MI)–superfluid transition(SF) of ultracold bosonic atoms or mixtures of bosons and fermions in deep optical lattices [Best *et al.*, Phys. Rev. Lett. **102**, 030408 (2009); Will *et al.*, Nature (London) **465**, 197 (2010)]. In the present work we derive an effective lowest-band Hamiltonian in three dimensions that generalizes the standard Bose-Fermi-Hubbard model taking these effects as well as nonlinear corrections of the tunneling amplitudes mediated by interspecies interactions into account. It is shown that a correct description of the lattice states in terms of the bare-lattice Wannier functions, rather than approximations such as harmonic-oscillator states, is essential. In contrast to self-consistent approaches based on effective Wannier functions, our approach captures the observed reduction of the superfluid phase for repulsive interspecies interactions.

DOI: 10.1103/PhysRevA.83.063630 PACS number(s): 03.75.Lm, 03.75.Mn, 37.10.Jk, 67.85.Pq

I. INTRODUCTION

Ultracold atoms in optical lattices provide unique and highly controllable realizations of various many-body Hamiltonians [1–6]. Theoretical descriptions of these systems in the case of deep-lattice potentials usually employ lowest-band models only [1,7]. However, it was found recently that for lattice bosons with a strong interaction contributions to the Hamiltonian beyond the single-band approximation with nearest-neighbor hopping and local two-particle interactions need to be taken into account [8]. For example, using the method of quantum phase diffusion, the value of the two-body interaction U for bosons in a deep optical lattice was measured directly and found to deviate from the prediction of the tight-binding model derived in Ref. [1]. These experiments also revealed the presence of additional local three- and four-body interactions not accounted for in the single-band Bose-Hubbard Hamiltonian. A perturbative derivation of these terms based on harmonic-oscillator approximations was given by Johnson *et al.* [9].

In the case of boson-fermion mixtures, the situation is more involved. Early experiments on mixtures with attractive interspecies interaction [10,11] displayed a decrease of the bosonic superfluidity in the presence of fermions. This initiated a controversial discussion about the nature of the effect. Explanations ranged from localization effects of bosons induced by fermions [11,12] to heating due to the admixture [10,13]. Numerical results also predicted the opposite behavior, i.e., the enhancement of bosonic superfluidity due to fermions [14] (for a more detailed discussion see Ref. [15]). The situation remained unclear until a systematic experimental study of the dependence of the shift in the bosonic superfluid–Mott-insulator (SF-MI) transition on the boson-fermion interaction [16] and the subsequent observation of higher-order interactions in the mixture. This shows that again higher-order band effects need to be taken into account.

The influence of higher Bloch bands in the Bose-Fermi mixture can be described by two different approaches. In the first approach one assumes that the single-particle Wannier functions are altered due to the modification of the lattice potential for one species by the interspecies interaction with the other [17], which is then calculated in a self-consistent manner. The agreement of these results with experimentally observed shifts of the SF-MI transition is very good for the case of the attractive boson-fermion interaction (see Ref. [16]). The method fails, however, for repulsive interactions where experiments showed (contrary to intuition again) a reduction of superfluidity [16]. Besides this shortcoming, the self-consistent potential approach has a conceptual weakness as it can only be applied close to the Mott-insulating phase. The second approach to include higher bands is an elimination scheme leading to an effective single-band Hamiltonian similar to the pure bosonic case [9,18,19]. This approach, although technically more involved, is more satisfactory from a fundamental point of view. However, so far, it has not resulted in quantitatively satisfactory predictions. We will show here that this is because (i) an important nonlinear correction to the hopping mediated by the interspecies interaction and present already in the absence of higher-band corrections is missing and (ii) harmonic-oscillator approximations to the Wannier functions that have been used before lead to gross errors when considering higher-band effects.

We present here an adiabatic elimination scheme for Bose-Fermi mixtures obtained independently from Refs. [9,18,19], resulting in an effective first-band Bose-Fermi-Hubbard Hamiltonian [20]. In contrast to Refs. [9,18,19], we use correct Wannier functions, which will be shown to be essential. Furthermore, we find that already within the lowest Bloch band the interspecies interaction leads to important nonlinear corrections to the tunneling matrix elements of bosons and fermions. For a fixed number of fermions per site, the effective Hamiltonian is equivalent to the Bose-Hubbard model with renormalized parameters U and J for which expressions are given in a closed form. This allows for a direct study of the influence of the boson-fermion interactions on the bosonic superfluid to Mott-insulator transition within this level of approximation. It is shown that nonlinear hopping together with higher-band corrections leads to a reduction of the bosonic superfluidity when adding fermions for both attractive and repulsive interspecies interactions.

The outline of the present work is as follows. After deriving the general multiband Hamiltonian of interacting spin-polarized fermions and bosons in a deep lattice in Sec. II, we introduce the first of two important additions to the standard Bose-Fermi-Hubbard model (BFHM) in Sec. III: the nonlinear hopping correction. By restricting the calculations to leading contributions, we derive an effective single-band Hamiltonian by adiabatic elimination of the higher bands in Sec. IV. Finally, using the resulting generalized BFHM, the effect of a varying boson-fermion interaction is studied in detail in Sec. V.

II. MODEL

In three dimensions, ultracold Bose-Fermi mixtures in an external potential are described by the continuous Hamiltonian [7]

$$\begin{aligned}\hat{H} = &\int d^3r\, \hat{\Psi}_b^\dagger(\mathbf{r})\left(-\frac{\hbar^2}{2m_b}\Delta + V^b(\mathbf{r})\right)\hat{\Psi}_b(\mathbf{r})\\ &+\int d^3r\, \hat{\Psi}_f^\dagger(\mathbf{r})\left(-\frac{\hbar^2}{2m_f}\Delta + V^f(\mathbf{r})\right)\hat{\Psi}_f(\mathbf{r})\\ &+\frac{g_{bb}}{2}\int d^3r\, \hat{\Psi}_b^\dagger(\mathbf{r})\hat{\Psi}_b^\dagger(\mathbf{r})\hat{\Psi}_b(\mathbf{r})\hat{\Psi}_b(\mathbf{r})\\ &+\frac{g_{bf}}{2}\int d^3r\, \hat{\Psi}_b^\dagger(\mathbf{r})\hat{\Psi}_f^\dagger(\mathbf{r})\hat{\Psi}_f(\mathbf{r})\hat{\Psi}_b(\mathbf{r}),\end{aligned} \tag{1}$$

where the index $b(f)$ on the field operators $\hat{\Psi}$ refers to bosonic (fermionic) quantities and $V^b(\mathbf{r})$ [$V^f(\mathbf{r})$] is the external potential consisting of possible trapping potentials as well as the optical lattice $V^b_{\mathrm{lat}}(\mathbf{r}) = \eta_b \sum \sin^2(k_\alpha r_\alpha)$ [$V^f_{\mathrm{lat}}(\mathbf{r}) = \eta_f \sum \sin^2(k_\alpha r_\alpha)$]. The intraspecies and interspecies interaction constants are defined as

$$g_{bb} = \frac{4\pi\hbar^2}{m_b}\, a_{bb}, \quad g_{bf} = \frac{4\pi\hbar^2}{m_R}\, a_{bf}, \tag{2}$$

with $m_R = \frac{m_b m_f}{m_b+m_f}$ being the reduced mass and $a_{bb/bf}$ the intraspecies and interspecies s-wave scattering lengths, respectively.

Whereas in the standard approach the field operators in Eq. (1) are expanded in terms of Wannier functions for the first band only, here we use an expansion to all Bloch bands:

$$\begin{aligned}\hat{\Psi}_b(\mathbf{r}) &= \sum_{\boldsymbol{\nu}}\sum_{\mathbf{j}} \hat{b}_{\boldsymbol{\nu},\mathbf{j}}\, w^b_{\boldsymbol{\nu}}(\mathbf{r}-\mathbf{j}),\\ \hat{\Psi}_f(\mathbf{r}) &= \sum_{\boldsymbol{\nu}}\sum_{\mathbf{j}} \hat{f}_{\boldsymbol{\nu},\mathbf{j}}\, w^f_{\boldsymbol{\nu}}(\mathbf{r}-\mathbf{j}).\end{aligned} \tag{3}$$

The operator $\hat{b}_{\boldsymbol{\nu},\mathbf{j}}$ ($\hat{f}_{\boldsymbol{\nu},\mathbf{j}}$) denotes the annihilation of a boson (fermion) in the $\boldsymbol{\nu}$th band at site $\mathbf{j}$ and $w^{b/f}_{\boldsymbol{\nu}}(\mathbf{r}-\mathbf{j})$ is the corresponding Wannier function of the $\boldsymbol{\nu}$th band located at site $\mathbf{j}$. The vector $\boldsymbol{\nu} = \{\nu_x,\nu_y,\nu_z\}$ denotes the band index. The Wannier functions factorize as

$$w^{b/f}_{\boldsymbol{\nu}}(\mathbf{r}) = \widetilde{w}^{b/f}_{\nu_x}(x)\, \widetilde{w}^{b/f}_{\nu_y}(y)\, \widetilde{w}^{b/f}_{\nu_z}(z), \tag{4}$$

with the one-dimensional Wannier function $\widetilde{w}^{b/f}_{\beta}(x)$.

Using the expansion of the field operator, the full multiband Bose-Fermi-Hubbard Hamiltonian can be expressed as

$$\begin{aligned}\hat{H} = &\sum_{\substack{\boldsymbol{\nu},\boldsymbol{\mu}\\ \mathbf{j}_1,\mathbf{j}_2}} \left(J^{\mathbf{j}_1,\mathbf{j}_2}_{\boldsymbol{\nu},\boldsymbol{\mu}}\, \hat{b}^\dagger_{\boldsymbol{\nu},\mathbf{j}_1}\hat{b}_{\boldsymbol{\mu},\mathbf{j}_2} + \widetilde{J}^{\mathbf{j}_1,\mathbf{j}_2}_{\boldsymbol{\nu},\boldsymbol{\mu}}\, \hat{f}^\dagger_{\boldsymbol{\nu},\mathbf{j}_1}\hat{f}_{\boldsymbol{\mu},\mathbf{j}_2}\right)\\ &+\frac{1}{2}\sum_{\substack{\boldsymbol{\nu},\boldsymbol{\mu},\boldsymbol{\varrho},\boldsymbol{\sigma}\\ \mathbf{j}_1,\ldots,\mathbf{j}_4}} \left(U^{\mathbf{j}_1,\ldots,\mathbf{j}_4}_{\boldsymbol{\nu},\boldsymbol{\mu},\boldsymbol{\varrho},\boldsymbol{\sigma}}\, \hat{b}^\dagger_{\boldsymbol{\nu},\mathbf{j}_1}\hat{b}^\dagger_{\boldsymbol{\mu},\mathbf{j}_2}\hat{b}_{\boldsymbol{\varrho},\mathbf{j}_3}\hat{b}_{\boldsymbol{\sigma},\mathbf{j}_4}\right)\\ &+\frac{1}{2}\sum_{\substack{\boldsymbol{\nu},\boldsymbol{\mu},\boldsymbol{\varrho},\boldsymbol{\sigma}\\ \mathbf{j}_1,\ldots,\mathbf{j}_4}} \left(V^{\mathbf{j}_1,\ldots,\mathbf{j}_4}_{\boldsymbol{\nu},\boldsymbol{\mu},\boldsymbol{\varrho},\boldsymbol{\sigma}}\, \hat{b}^\dagger_{\boldsymbol{\nu},\mathbf{j}_1}\hat{b}_{\boldsymbol{\mu},\mathbf{j}_2}\hat{f}^\dagger_{\boldsymbol{\varrho},\mathbf{j}_3}\hat{f}_{\boldsymbol{\sigma},\mathbf{j}_4}\right).\end{aligned} \tag{5}$$

The generalized hopping amplitudes (still containing local energy contributions)

$$\begin{aligned}J^{\mathbf{j}_1,\mathbf{j}_2}_{\boldsymbol{\nu},\boldsymbol{\mu}} = &\int d^3r\, \bar{w}^b_{\boldsymbol{\nu}}(\mathbf{r}-\mathbf{j}_1)\\ &\times\left(-\frac{\hbar^2}{2m_b}\Delta + V^b(\mathbf{r})\right) w^b_{\boldsymbol{\mu}}(\mathbf{r}-\mathbf{j}_2),\end{aligned} \tag{6}$$

$$\begin{aligned}\widetilde{J}^{\mathbf{j}_1,\mathbf{j}_2}_{\boldsymbol{\nu},\boldsymbol{\mu}} = &\int d^3r\, \bar{w}^f_{\boldsymbol{\nu}}(\mathbf{r}-\mathbf{j}_1)\\ &\times\left(-\frac{\hbar^2}{2m_f}\Delta + V^f(\mathbf{r})\right) w^f_{\boldsymbol{\mu}}(\mathbf{r}-\mathbf{j}_2)\end{aligned} \tag{7}$$

and the generalized interaction amplitudes

$$\begin{aligned}U^{\mathbf{j}_1,\mathbf{j}_2,\mathbf{j}_3,\mathbf{j}_4}_{\boldsymbol{\nu},\boldsymbol{\mu},\boldsymbol{\varrho},\boldsymbol{\sigma}} = g_{bb}&\int d^3r\, \bar{w}^b_{\boldsymbol{\nu}}(\mathbf{r}-\mathbf{j}_1)\\ &\times \bar{w}^b_{\boldsymbol{\mu}}(\mathbf{r}-\mathbf{j}_2) w^b_{\boldsymbol{\varrho}}(\mathbf{r}-\mathbf{j}_3) w^b_{\boldsymbol{\sigma}}(\mathbf{r}-\mathbf{j}_4),\end{aligned} \tag{8}$$

$$\begin{aligned}V^{\mathbf{j}_1,\mathbf{j}_2,\mathbf{j}_3,\mathbf{j}_4}_{\boldsymbol{\nu},\boldsymbol{\mu},\boldsymbol{\varrho},\boldsymbol{\sigma}} = g_{bf}&\int d^3r\, \bar{w}^b_{\boldsymbol{\nu}}(\mathbf{r}-\mathbf{j}_1)\\ &\times w^b_{\boldsymbol{\mu}}(\mathbf{r}-\mathbf{j}_2) \bar{w}^f_{\boldsymbol{\varrho}}(\mathbf{r}-\mathbf{j}_3) w^f_{\boldsymbol{\sigma}}(\mathbf{r}-\mathbf{j}_4)\end{aligned} \tag{9}$$

are defined as usual. In the following we restrict our model in such a way that only the most relevant terms are kept. Note that many of the matrix elements vanish because of the symmetry of the Wannier functions [21]. Unless stated otherwise, we restrict ourselves to local contributions in the interaction terms, i.e., $\mathbf{j}_1 = \cdots = \mathbf{j}_4$ in $U^{\mathbf{j}_1,\ldots,\mathbf{j}_4}_{\boldsymbol{\nu},\boldsymbol{\mu},\boldsymbol{\varrho},\boldsymbol{\sigma}}$ and $V^{\mathbf{j}_1,\ldots,\mathbf{j}_4}_{\boldsymbol{\nu},\boldsymbol{\mu},\boldsymbol{\varrho},\boldsymbol{\sigma}}$, and in this case we drop the site indices.

With these restrictions, the general multiband Hamiltonian can be cast in the form

$$\hat{H} = \hat{H}_{\mathbf{1}} + \sum_{\boldsymbol{\nu}\neq\mathbf{1}} \hat{H}^0_{\boldsymbol{\nu}} + {\sum_{\boldsymbol{\nu},\boldsymbol{\mu},\boldsymbol{\varrho},\boldsymbol{\sigma}}}' \hat{H}_{\boldsymbol{\nu}\boldsymbol{\mu}\boldsymbol{\varrho}\boldsymbol{\sigma}}, \tag{10}$$

where the first term

$$\hat{H}_{\mathbf{1}} = \hat{H}_{\mathrm{BFHM}} + \hat{H}_{\mathrm{nl}} \tag{11}$$

describes the (pure) first-band ($\mathbf{1} = \{1,1,1\}$) dynamics consisting of the standard Bose-Fermi-Hubbard–model part $\hat{H}_{\mathrm{BFHM}}$ [7] and nonlinear hopping corrections $\hat{H}_{\mathrm{nl}}$, which will be discussed in Sec. III. The second term $\hat{H}^0_{\boldsymbol{\nu}}$ incorporates the (free) dynamics within the $\boldsymbol{\nu}$th band and $\hat{H}_{\boldsymbol{\nu}\boldsymbol{\mu}\boldsymbol{\varrho}\boldsymbol{\sigma}}$ describes

the coupling between arbitrary bands $\boldsymbol{\nu},\boldsymbol{\mu},\boldsymbol{\varrho},\boldsymbol{\sigma}$. The prime in the sum indicates that at least one multi-index has to be different from the others. This general form of the full Hamiltonian serves as the starting point of our study.

III. NONLINEAR HOPPING CORRECTION

Even when virtual transitions to higher bands are disregarded there are important corrections to the standard BFHM if the boson-fermion interaction V becomes large. The interspecies interaction term in Eq. (1) gives rise to a correction to the bosonic (and fermionic) tunneling amplitude proportional to the occupation number of the corresponding complementary species. These contributions (in the following referred to as nonlinear hopping contributions) have been considered before [22,23], but have been omitted from earlier discussions of corrections to the BFHM [18,19].

To establish notation let us recall first the usual single-band BFHM

$$\hat{H} = -J \sum_{\langle \mathbf{ij} \rangle} \hat{b}_{\mathbf{i}}^{\dagger} \hat{b}_{\mathbf{j}} + \frac{U}{2} \sum_{\mathbf{j}} \hat{n}_{\mathbf{j}}(\hat{n}_{\mathbf{j}} - 1) - \tilde{J} \sum_{\langle \mathbf{ij} \rangle} \hat{f}_{\mathbf{i}}^{\dagger} \hat{f}_{\mathbf{j}} + \frac{V}{2} \sum_{\mathbf{j}} \hat{n}_{\mathbf{j}} \hat{m}_{\mathbf{j}}. \tag{12}$$

The amplitudes are determined by

$$U \equiv U_{\mathbf{1111}}^{\mathbf{iiii}}, \quad V \equiv V_{\mathbf{1111}}^{\mathbf{iiii}}, \quad J \equiv -J_{\mathbf{1,1}}^{\mathbf{i+\hat{e},i}}, \quad \tilde{J} \equiv -\tilde{J}_{\mathbf{1,1}}^{\mathbf{i+\hat{e},i}},$$

with $\hat{\mathbf{e}}$ being a unit vector in one of the three lattice directions. Due to the isotropic setup, the choice of direction is irrelevant. From Eqs. (8) and (9) two types of nonlinear hopping corrections arise: From the boson-boson interaction we obtain

$$J_{\mathrm{nl}}^{b} \sum_{\langle \mathbf{ij} \rangle} \hat{b}_{\mathbf{i}}^{\dagger}(\hat{n}_{\mathbf{i}} + \hat{n}_{\mathbf{j}}) \hat{b}_{\mathbf{j}}, \tag{13}$$

whereas the boson-fermion interaction leads to both bosonic and fermionic hopping corrections:

$$J_{\mathrm{nl}}^{f} \sum_{\langle \mathbf{ij} \rangle} \hat{b}_{\mathbf{i}}^{\dagger}(\hat{m}_{\mathbf{i}} + \hat{m}_{\mathbf{j}}) \hat{b}_{\mathbf{j}} + \tilde{J}_{\mathrm{nl}} \sum_{\langle \mathbf{ij} \rangle} \hat{f}_{\mathbf{i}}^{\dagger}(\hat{n}_{\mathbf{i}} + \hat{n}_{\mathbf{j}}) \hat{f}_{\mathbf{j}}. \tag{14}$$

The corresponding nonlinear hopping amplitudes read

$$J_{\mathrm{nl}}^{b} \equiv U_{\mathbf{1111}}^{\mathbf{j+\hat{e},j,j,j}}, \quad J_{\mathrm{nl}}^{f} \equiv V_{\mathbf{1111}}^{\mathbf{j+\hat{e},j,j,j}}, \quad \tilde{J}_{\mathrm{nl}} \equiv V_{\mathbf{1111}}^{\mathbf{j,j,j+\hat{e},j}}.$$

Since we are interested in the influence of the fermions on the bosons we assume in the following the fermions to be homogeneously distributed. This assumption, also used in Refs. [16,17], proved to be valid in the trap center and provides a considerable simplification. This amounts to replacing the fermionic number operators by the fermionic filling: $\hat{m}_{\mathbf{j}} \to m$. Furthermore, the bosonic density operators in Eqs. (13) and (14) are replaced by the filling of the Mott lobe under consideration, $\hat{n}_{\mathbf{j}} \to n$, for simplicity.

Altogether, this allows us to write a Hamiltonian including corrections from the nonlinear hopping contributions. By defining the effective bosonic hopping amplitude as

$$J[n,m] \equiv J - 2n\, J_{\mathrm{nl}}^{b} - m J_{\mathrm{nl}}^{f}, \tag{15}$$

the system is recast in the form of a pure Bose-Hubbard model (BHM) with density-dependent hopping:

$$\hat{H}_{\mathrm{eff}} = -J[n,m] \sum_{\langle \mathbf{ij} \rangle} \hat{a}_{\mathbf{i}}^{\dagger} \hat{a}_{\mathbf{j}} + \frac{U}{2} \sum_{\mathbf{j}} \hat{n}_{\mathbf{j}}(\hat{n}_{\mathbf{j}} - 1). \tag{16}$$

By analyzing the resulting predictions for the MI-SF transition as a function of the filling and the interspecies interaction (see Fig. 3) one recognizes a substantial reduction of bosonic superfluidity for increasing interaction on the attractive side and a corresponding enhancement on the repulsive side, showing the importance of nonlinear hopping terms for the precise determination of the MI-SF transition. Compared to the experimental results [16], two main points arise. First, although pointing in the right direction for attractive interactions, the overall shift is too small compared to the experimental observation. Second, for repulsive interactions, the transition is shifted to larger lattice depths, in contrast to the experimental findings.

IV. EFFECTIVE SINGLE-BAND HAMILTONIAN

In the following we derive an effective single-band Hamiltonian that takes into account the coupling to higher bands. The derivation is structured in the following way. We use an adiabatic elimination scheme presented in Appendix A, which reduces the main task to the calculation of the second-order cumulant $\langle\langle \mathcal{T} H_I(\tau + T) H_I(\tau) \rangle\rangle$ in the interaction picture, where the average is taken over the higher bands. The full interaction Hamiltonian $\hat{H}_I = \sum'_{\boldsymbol{\nu},\boldsymbol{\mu},\boldsymbol{\varrho},\boldsymbol{\sigma}} \hat{H}_{\boldsymbol{\nu}\boldsymbol{\mu}\boldsymbol{\varrho}\boldsymbol{\sigma}}$ is then reduced according to the relevant contributions of the cumulant. Finally, a reduction of the effective bosonic scattering matrix [Eq. (A5)] gives the full effective single-band Bose-Fermi-Hubbard model.

When calculating the cumulant $\langle\langle \mathcal{T} H_I(\tau + T) H_I(\tau) \rangle\rangle$ in Eq. (A5), the interaction Hamiltonian of the full multiband Bose-Fermi-Hubbard model can be reduced considerably. Keeping only terms that lead to nonzero contributions in lowest order, it is easy to see that only those terms in $\hat{H}_I$ matter, where particles are transferred to higher bands by $\hat{H}_I(\tau)$ and down again by $\hat{H}_I(\tau + T)$. In the following we restrict ourselves to precisely those contributions and furthermore treat only local contributions since these are dominant. Three relevant processes are found. (i) The contributions from single-particle transitions to a certain band $\boldsymbol{\nu}$, $\{\mathbf{1},\mathbf{1},\mathbf{1},\mathbf{1}\} \leftrightarrow \{\boldsymbol{\nu},\mathbf{1},\mathbf{1},\mathbf{1}\}$, can be understood as density-mediated band transitions, where the matrix elements $U_{\boldsymbol{\nu}\mathbf{111}}$, $V_{\boldsymbol{\nu}\mathbf{111}}$, and $V_{\mathbf{1}\boldsymbol{\nu}\mathbf{11}}$ are only nonzero for odd bands $\boldsymbol{\nu}$ [24]. Note that from now on, the upper site indices are omitted if they are all the same. (ii) In the situation with double-particle transitions to the same band $\boldsymbol{\nu}$, $\{\mathbf{1},\mathbf{1},\mathbf{1},\mathbf{1}\} \leftrightarrow \{\boldsymbol{\nu},\boldsymbol{\nu},\mathbf{1},\mathbf{1}\}$, two particles undergo a transition to the same band and all bands are incorporated. The matrix elements are $U_{\boldsymbol{\nu}\boldsymbol{\nu}\mathbf{11}}$ and $V_{\boldsymbol{\nu}\boldsymbol{\nu}\mathbf{11}}$. (iii) In the combined process of double-particle transitions to different bands $\boldsymbol{\nu}$ and $\boldsymbol{\mu}$, $\{\mathbf{1},\mathbf{1},\mathbf{1},\mathbf{1}\} \leftrightarrow \{\boldsymbol{\nu},\boldsymbol{\mu},\mathbf{1},\mathbf{1}\}$, the two different bands both have to be either even or odd with matrix elements $U_{\boldsymbol{\nu}\boldsymbol{\mu}\mathbf{11}}$ and $V_{\boldsymbol{\nu}\boldsymbol{\mu}\mathbf{11}}$.

The remaining important contributions to the full multiband BFHM result from the kinetic energy of the particles. By restricting the contributions to the usual nearest-neighbor hoppings within a given Bloch band ($\boldsymbol{\nu} = \boldsymbol{\mu}$ and $|\mathbf{j}_1 - \mathbf{j}_2| = 1$)

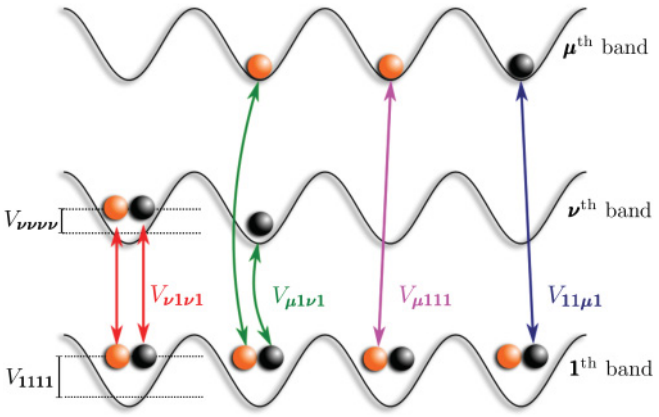

FIG. 1. (Color online) Matrix elements for the coupling of the higher Bloch bands to the first band via the generalized interaction in Eq. (9). Bosonic contributions from Eq. (8) are equivalent. Bosons are shown as orange circles and fermions in black. $V_{\nu 1\nu 1}$ describes the transition of a boson and a fermion from the first (higher) to the higher (first) band; $V_{\mu 1\nu 1}$ gives two particles (boson and fermion), which perform a transition to bands ν and μ. $V_{\mu 111}$ describes a fermion-mediated single-particle transition of a boson, where $V_{11\mu 1}$ is a boson-mediated transition of a fermion.

and the energy of the particles within a band ($\nu = \mu$ and $\mathbf{j}_1 = \mathbf{j}_2$), these are (iv) the band energies Δ_ν^b and Δ_ν^f and (v) the intraband nearest-neighbor hopping for bosons J_ν and, correspondingly, for fermions $\widetilde{J}_\nu$. Hopping between sites with $|\mathbf{j}_1 - \mathbf{j}_2| \neq 1$ is omitted since it is unimportant. In Appendix B the different contributions to the Hamiltonian as well as the hoppings and band energies are defined in detail. Figure 1 gives a sketch of the different contributions taken into account. Only processes involving fermions are shown.

From the effective bosonic scattering matrix in Eq. (A5), the effective single-band BFHM is derived by applying a Markov approximation [25]. This amounts to replacing first-band operators at time $\tau + T$ by the corresponding operators at time τ, which is valid since the time scale of the higher-band dynamics is much shorter than in the first band because of the larger hopping amplitude [26]. The resulting Hamiltonian is lengthy and is given in Appendix C.

The effective Hamiltonian [Eq. (C1)] contains nonlocal interaction and long-range tunneling terms. These result from virtual transitions into higher bands and subsequent tunneling processes in these bands. As these terms rapidly decrease with increasing distance $|\mathbf{d}|$ between the involved lattice sites, it is sufficient to take into account only the leading-order contributions, i.e., only local interaction terms ($|\mathbf{d}| = 0$) and only nearest-neighbor hopping ($|\mathbf{d}| = \pm 1$). This leads to the following extensions compared to the standard single-band BFHM:

$$\hat{H}^{\text{eff}} = \sum_{\mathbf{j}} \left(\frac{U_3}{6}\, \hat{n}_{\mathbf{j}}(\hat{n}_{\mathbf{j}} - 1)(\hat{n}_{\mathbf{j}} - 2) + \frac{V_3}{2}\, \hat{m}_{\mathbf{j}}\hat{n}_{\mathbf{j}}(\hat{n}_{\mathbf{j}} - 1) + \frac{U_2}{2}\hat{n}_{\mathbf{j}}(\hat{n}_{\mathbf{j}} - 1) + \frac{V_2}{2}\hat{n}_{\mathbf{j}}\hat{m}_{\mathbf{j}} \right) + \sum_{\mathbf{j}} \Delta_{\mathbf{1}}^b \hat{n}_{\mathbf{j}} + \sum_{\mathbf{j}} \Delta_{\mathbf{1}}^b \hat{m}_{\mathbf{j}}$$
$$- \sum_{\langle \mathbf{ij} \rangle} \hat{b}_{\mathbf{i}}^\dagger\, J[\hat{n}_{\mathbf{i}}, \hat{n}_{\mathbf{j}}, \hat{m}_{\mathbf{i}}, \hat{m}_{\mathbf{j}}]\, \hat{b}_{\mathbf{j}} - \sum_{\langle \mathbf{ij} \rangle} \hat{f}_{\mathbf{i}}^\dagger\, \widetilde{J}[\hat{n}_{\mathbf{i}}, \hat{n}_{\mathbf{j}}]\, \hat{f}_{\mathbf{j}}$$
$$+ \sum_{\langle \mathbf{ij} \rangle} \left[J^{(2)} (\hat{b}_{\mathbf{i}}^\dagger)^2 \hat{b}_{\mathbf{j}}^2 + \widetilde{J}^{(2)}\, \hat{b}_{\mathbf{i}}^\dagger \hat{f}_{\mathbf{i}}^\dagger \hat{f}_{\mathbf{j}} \hat{b}_{\mathbf{j}} \right]. \tag{17}$$

Compared to the standard BHM, several further terms arise, for instance, the correlated two-particle tunneling terms $J^{(2)}$ and $\widetilde{J}^{(2)}$. Most prominent is the appearance of the three-body interactions U_3 and V_3. The bosonic interaction U_3 has recently been measured by means of quantum phase diffusion [8]. It should be noted that in the experiments in Ref. [8] higher-order nonlinear interactions also were detected. However, since our approach is only second order in the interaction-induced intraband coupling, these terms cannot be reproduced. In addition to the terms beyond the standard BHM, the higher bands lead to a renormalization of the usual single-band BFHM parameters. Whereas the local two-body interaction amplitudes U_2 and V_2 depend only on the band structure, the hopping amplitudes are altered, leading to density-mediated hopping processes. For the bosonic amplitudes, the hopping now is of the form

$$J[\hat{n}_{\mathbf{i}}, \hat{n}_{\mathbf{j}}, \hat{m}_{\mathbf{i}}, \hat{m}_{\mathbf{j}}] = J - J_{\text{nl}}^b(\hat{n}_{\mathbf{j}} + \hat{n}_{\mathbf{i}}) - \frac{J_{\text{nl}}^f}{2}\, (\hat{m}_{\mathbf{j}} + \hat{m}_{\mathbf{i}}) + \alpha \hat{n}_{\mathbf{i}}\hat{n}_{\mathbf{j}} + \beta \hat{m}_{\mathbf{i}}\hat{n}_{\mathbf{j}} + \gamma \hat{n}_{\mathbf{i}}\hat{m}_{\mathbf{j}} + \delta \hat{m}_{\mathbf{i}}\hat{m}_{\mathbf{j}} \tag{18}$$

and the density dependence is directly seen. For all parameters occurring in Eq. (17), full expressions can be found in Appendix D.

V. INFLUENCE OF FERMIONS ON THE BOSONIC MI-SF TRANSITION

In order to discuss the phase transition of the bosonic subsystem, we make further approximations. Coming from the Mott-insulator side of the phase transition, the local number of bosons is approximately given by the integer average filling, i.e., $\langle \hat{n}_{\mathbf{j}} \rangle \approx n$. For the fermionic species, we also replace the number operator by the average fermion number $\hat{m}_{\mathbf{j}} \to m = 1$, assuming a homogeneous filling of fermions in the lattice. If we have an experimental realization with cold atoms in mind, this is a valid assumption in the center of the harmonic trap at least for attractive interspecies interactions. It should also be valid, however, for slight interspecies repulsion. This assumption is also supported by the results of Ref. [16], where the actual fermionic density did not influence the transition from a Mott insulator to a superfluid (for medium and large fillings). It also agrees with the result in Ref. [17], which is based on this assumption and shows good agreement with the experimental results. All further contributions to the Hamiltonian, such as the bosonic three-particle interaction and two-particle hoppings, are neglected in the following. With these approximations, the renormalized Bose-Hubbard Hamiltonian for the nth Mott lobe with mean fermionic filling m can be written as

$$\hat{H}^{\text{eff}} = -J[n,m] \sum_{\langle \mathbf{ij} \rangle} \hat{b}_{\mathbf{i}}^\dagger \hat{b}_{\mathbf{j}} + \frac{U[m]}{2} \sum_{\mathbf{j}} \hat{n}_{\mathbf{j}}(\hat{n}_{\mathbf{j}} - 1), \tag{19}$$

with

$$J[n,m] = J - 2nJ^b_{\rm nl} - mJ^f_{\rm nl} - \sum_{\boldsymbol{\nu}\neq\mathbf{1}} \mathcal{I}^{\hat{\mathbf{e}}}_{b,\boldsymbol{\nu}} \left(U_{\boldsymbol{\nu}\mathbf{111}}\, n + V_{\boldsymbol{\nu}\mathbf{111}} \frac{m}{2}\right)^2, \tag{20}$$

$$U[m] = U_2 + mV_3. \tag{21}$$

The final form of the bosonic Hamiltonian will now be used to discuss the influence of the boson-fermion interaction on the MI-SF transition. Following the experimental procedure presented in Ref. [16], we consider the shift of the bosonic transition as a function of the boson-fermion interaction determined by the scattering length a_{BF}, with special emphasis on the repulsive interaction, where no theoretical prediction exists so far.

To determine the transition point, we calculate the bosonic hopping [Eq. (20)] and interaction amplitude [Eq. (21)] using numerically determined Wannier functions. Knowledge of the critical ratio U/J of the MI-SF transition from analytic or numerical results [27–29] allows for the precise localization of the transition point [30]. This method is displayed in Fig. 2, where the ratio of the effective interaction strength $U[1]$ to the effective tunneling rate $J[1,1]$ as per Eqs. (20) and (21) is plotted as a function of the normalized lattice depth η_b, which describes the amplitude of the periodic lattice potential of the bosons $V^b_{\rm lat}$ in units of the recoil energy of the bosons $E^b_{\rm rec} = \hbar^2\mathbf{k}^2/2m_b$. As indicated, unity fermion filling $m = 1$ is assumed and the bosonic Mott lobe with $n = 1$ is considered. The horizontal dotted line gives the critical value for the MI-SF transition [27] and the crossing of this line with the different curves, which illustrate the relative contribution of the various correction terms, determines the potential depth at which the phase transition occurs. The different levels of approximation shown in Fig. 2 are (i) harmonic oscillator, which uses the plain BHM and the harmonic-oscillator approximation; (ii) pure bosonic, which uses the plain BHM and proper Wannier functions; (iii) nonlinear bosonic, which uses the BHM extended by the nonlinear (bosonic) hopping correction; (iv) nonlinear bosonic with higher bands, which includes all bands with $\nu_\alpha \leqslant 25$ and gives the reference point for the shift of the transition; (v) and nonlinear bosonic and fermionic with higher bands, which includes fermions, the nonlinear hopping correction, and higher bands ($\nu_\alpha \leqslant 25$). A substantial shift of the transition point to lower potential depth is easily recognizable, in qualitative agreement with the experiment. It is also apparent that using harmonic-oscillator approximations leads to a large error of the predicted transition point. This shows that the use of the correct Wannier functions is crucial for obtaining reliable predictions.

Figure 3 shows the shift of the MI-SF transition point for the first four lobes as a function of the boson-fermion scattering length a_{bf}. The solid lines include all corrections described earlier, where the amount of the shift is measured relative to the nonlinear bosonic case including higher bands, i.e., relative to the real bosonic transition point. Thus the figure corresponds to the shift of the transition point when fermions with unity filling are added to the system. For each Mott lobe three curves are shown corresponding to different ratios of η_f/η_b, which illustrates the effect of different masses and/or different polarizabilities of the bosonic and fermionic species as discussed in Appendix E. The dash-dotted curves give the contributions of the (first-band) nonlinear hopping corrections only (bosons and fermions). It is clear that for increasingly attractive interactions between the species there is an increasing shift of the transition point toward smaller potential depth, corresponding to a reduction of bosonic superfluidity in the presence of fermions.

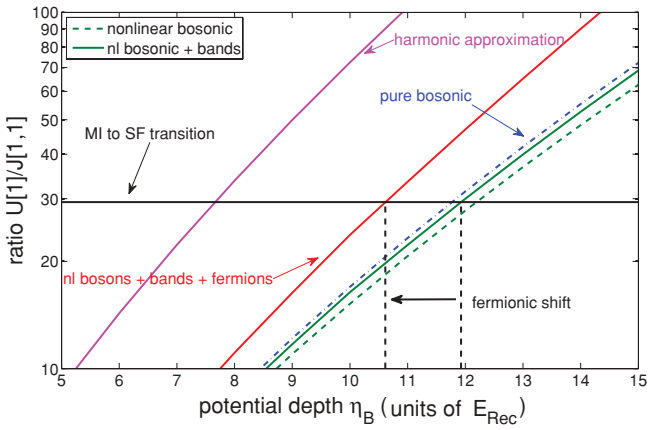

FIG. 2. (Color online) Ratio of effective interaction U to effective tunneling rate J for unity fermion filling $m = 1$ and Mott lobe with $n = 1$ as a function of normalized lattice depth η_b for the bosons and for the attractive boson-fermion interaction with a scattering length $a_{bf} = -400a_0$. The horizontal dotted line gives the critical value for the MI-SF transition point in the Bose-Hubbard model. The harmonic-oscillator approximation is shown together with different levels of corrections, as described in the main text, based on exact Wannier functions. A perfect match is assumed between fermionic and bosonic Wannier functions, $\eta_F \equiv \eta_B$.

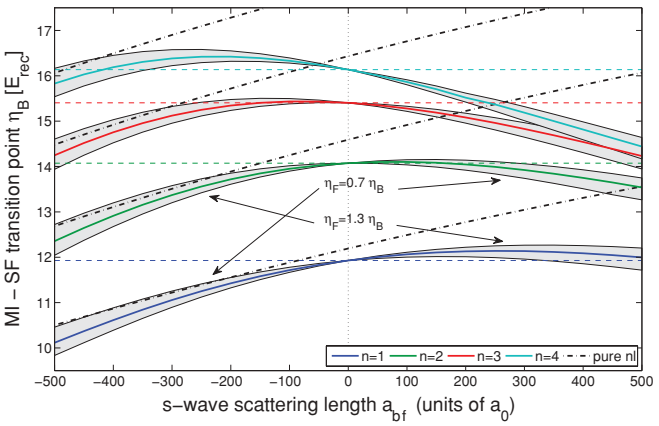

FIG. 3. (Color online) Shift of the bosonic MI-SF transition as a function of the boson-fermion scattering length a_{bf} for different Mott lobes (solid lines, $n = 1, \ldots, 4$, from bottom to top) in one dimension. The gray-shaded region depicts the influence of a mismatch of the bosonic and fermionic lattice depths. The dash-dotted lines give the shifts of the transition solely from the nonlinear tunneling corrections. Dashed horizontal lines give the transition points for the pure bosonic system.

Interestingly, it is clear that for repulsive interspecies interactions, virtual transitions to higher Bloch bands tend to counteract the effect of the fermion-induced nonlinear tunneling. For larger values of n there is again a shift of the MI-SF transition point toward smaller lattice depth, i.e., again a reduction of bosonic superfluidity. The latter effect has been observed in the experiments [16], but is not yet fully understood. In the calculations, the bands are summed up to a maximal multi-index $\boldsymbol{\nu}_{\max} = \{25,25,25\}$, including altogether 15 625 bands. For this number of bands, a satisfactory convergence of the effective amplitudes U and J is found. Overall, our second-order approach including the nonlinear corrections provides an intuitive explanation for the behavior of the system in the experiment. This especially holds for the repulsive case, where the agreement with the experimental results is on a quantitative level.

VI. CONCLUSION

In the present paper we studied the influence of nonlinear tunneling processes and higher Bloch bands on the dynamics of a mixture of bosons and fermions in a deep optical lattice in a full three-dimensional setup. By taking into account virtual interband transitions in lowest nonvanishing order and contributions of the originally continuous interaction to tunneling processes we derived an effective lowest-band Hamiltonian, thereby extending the standard Bose-Fermi-Hubbard model. This Hamiltonian contains interaction-mediated nonlinear corrections to the tunneling rates, renomalized two-body interactions, and effective three-body interaction terms. We showed that an accurate determination of the effective model parameter requires the use of the correct Wannier functions of the corresponding single-particle model. As differences in the tails of the wave functions are essential, the use of approximate harmonic-oscillator wave functions can lead to large errors. The effective model allows for a study of the effect of admixing spin-polarized fermionic atoms to the bosonic superfluid–Mott-insulator transition when changing the boson-fermion interaction strength. Our model qualitatively recovers all features observed in the experiment. In particular we found that boson superfluidity is reduced for both attractive and repulsive interspecies interactions. The latter has not yet been reproduced with other methods, such as the self-consistent potential approach.

It should be noted that our model does not take into account heating effects and effects such as phase separation due to the presence of an inhomogeneous trapping potential, which have recently been shown to significantly affect the MI-SF transition point already in the lowest band [31,32]. We thus expect that a complete picture of the experimental observations will require proper inclusion of higher-band effects and nonlinear tunneling as derived in the present paper, as well as effects from heating and a trapping potential. Finally, it should be mentioned that our approach is limited to the second order in intraband processes. In higher-order perturbation theory effective four-body, five-body, etc., interactions will arise, which, however, play a progressively less important role. Nevertheless, we expect that the higher orders should substantially improve the results, especially for repulsive interactions.

ACKNOWLEDGMENTS

The authors thank S. Das Sarma, I. Bloch, and E. Demler for useful discussions. Financial support by the Deutsche Forschungsgemeinschaft through the SFB-TR49 is gratefully acknowledged.

APPENDIX A: ADIABATIC ELIMINATION SCHEME

As long as the interaction energies U and V and the temperature are small compared to the band gap between the lowest and first excited Bloch band, the population of higher bands can be neglected. However, as noted before, there are virtual transitions to higher bands that need to be taken into account. In the following we employ an adiabatic elimination scheme of higher Bloch bands starting from the general multiband Hamiltonian [Eq. (10)]. This scheme, which is also used in Ref. [33] for the Bose-Fermi-Hubbard model in the ultrafast-fermion limit, is equivalent to degenerate perturbation theory [27,34] and allows for a proper description of the reduced system. For this, the Hamiltonian [Eq. (10)] is split up into a free and an interaction part $\hat{H} = \hat{H}_{\text{free}} + \hat{H}_I$, with

$$\hat{H}_{\text{free}} = \hat{H}_{\mathbf{1}} + \sum_{\boldsymbol{\nu}\neq\mathbf{1}} \hat{H}^0_{\boldsymbol{\nu}}, \tag{A1}$$

$$\hat{H}_I = \sum_{\boldsymbol{\nu},\boldsymbol{\mu},\boldsymbol{\varrho},\sigma}{}' \hat{H}_{\boldsymbol{\nu},\boldsymbol{\mu},\boldsymbol{\varrho},\sigma}. \tag{A2}$$

Upon transformation to the interaction picture, the dynamics of the free part is incorporated by the time-dependent interaction Hamiltonian $H_I(\tau) = e^{-[(i/\hbar)H_{\text{free}}\tau]} H_I \; e^{[(i/\hbar)H_{\text{free}}\tau]}$. Adiabatic elimination is carried out for the time-evolution operator (scattering matrix) of the full system given by

$$\mathcal{S} = \mathcal{T} \exp\left(-\frac{i}{\hbar}\int_{-\infty}^{\infty} d\tau\, \hat{H}_I(\tau)\right). \tag{A3}$$

We now trace out the higher-band degrees of freedom, assuming empty higher bands. By using Kubo's cumulant expansion [35]

$$\langle \exp\{sX\}\rangle_X = \exp\left(\sum_{m=1}^{\infty} \frac{s^m}{m!} \langle\langle X^m \rangle\rangle\right) \tag{A4}$$

up to second order in the interband coupling, the effective scattering matrix for the lowest band reads

$$\mathcal{S}_{\text{eff}} = \mathcal{T} \exp\left[+ \frac{1}{2}\left(-\frac{i}{\hbar}\right)^2 \int_{-\infty}^{\infty} d\tau \int_{-\infty}^{\infty} dT \times \langle\langle \mathcal{T} H_I(\tau + T) H_I(\tau)\rangle\rangle\right]. \tag{A5}$$

The first order does not lead to any contributions because of the vacuum in the higher bands and due to the nature

of the interband couplings. Obviously, the effective bosonic Hamiltonian is connected to the second-order cumulants of operators in higher Bloch bands, $\langle\langle \hat{A}\hat{B}\rangle\rangle = \langle \hat{A}\hat{B}\rangle - \langle\hat{A}\rangle\langle\hat{B}\rangle$ [35].

APPENDIX B: RELEVANT BAND-COUPLING PROCESSES

As discussed in Sec. IV, the different terms contributing to the Hamiltonian are given by single-particle transitions to a certain band $\boldsymbol{\nu}$,

$$\frac{1}{2}\sum_{\mathbf{j}}\big(U_{\nu 111}\hat{b}_{\mathbf{1}}^{\dagger}\hat{b}_{\mathbf{1}}\hat{b}_{\nu}^{\dagger}\hat{b}_{\mathbf{1}} + U_{\mathbf{1}\nu 11}\hat{b}_{\mathbf{1}}^{\dagger}\hat{b}_{\mathbf{1}}\hat{b}_{\nu}^{\dagger}\hat{b}_{\mathbf{1}} + U_{11\nu 1}\hat{b}_{\mathbf{1}}^{\dagger}\hat{b}_{\nu}\hat{b}_{\mathbf{1}}^{\dagger}\hat{b}_{\mathbf{1}} + U_{111\nu}\hat{b}_{\mathbf{1}}^{\dagger}\hat{b}_{\nu}\hat{b}_{\mathbf{1}}^{\dagger}\hat{b}_{\mathbf{1}} + V_{\nu 111}\hat{b}_{\nu}^{\dagger}\hat{b}_{\mathbf{1}}\hat{f}_{\mathbf{1}}^{\dagger}\hat{f}_{\mathbf{1}} + V_{\mathbf{1}\nu 11}\hat{b}_{\mathbf{1}}^{\dagger}\hat{b}_{\nu}\hat{f}_{\mathbf{1}}^{\dagger}\hat{f}_{\mathbf{1}} + V_{11\nu 1}\hat{b}_{\mathbf{1}}^{\dagger}\hat{b}_{\mathbf{1}}\hat{f}_{\nu}^{\dagger}\hat{f}_{\mathbf{1}} + V_{111\nu}\hat{b}_{\mathbf{1}}^{\dagger}\hat{b}_{\mathbf{1}}\hat{f}_{\mathbf{1}}^{\dagger}\hat{f}_{\nu}\big); \tag{B1}$$

double-particle transitions to the same band $\boldsymbol{\nu}$,

$$\frac{1}{2}\sum_{\mathbf{j}}\big(U_{\nu\nu 11}\hat{b}_{\nu}^{\dagger}\hat{b}_{\nu}^{\dagger}\hat{b}_{\mathbf{1}}\hat{b}_{\mathbf{1}} + U_{11\nu\nu}\hat{b}_{\mathbf{1}}^{\dagger}\hat{b}_{\mathbf{1}}^{\dagger}\hat{b}_{\nu}\hat{b}_{\nu} + V_{\nu 1\nu 1}\hat{b}_{\nu}^{\dagger}\hat{b}_{\mathbf{1}}\hat{f}_{\nu}^{\dagger}\hat{f}_{\mathbf{1}} + V_{\mathbf{1}\nu 1\nu}\hat{b}_{\mathbf{1}}^{\dagger}\hat{b}_{\nu}\hat{f}_{\mathbf{1}}^{\dagger}\hat{f}_{\nu}\big); \tag{B2}$$

and double-particle transitions to different bands $\boldsymbol{\nu}$ and $\boldsymbol{\mu}$,

$$\frac{1}{2}\sum_{\mathbf{j}}\big(U_{\nu\mu 11}\hat{b}_{\nu}^{\dagger}\hat{b}_{\mu}^{\dagger}\hat{b}_{\mathbf{1}}\hat{b}_{\mathbf{1}} + U_{11\nu\mu}\hat{b}_{\mathbf{1}}^{\dagger}\hat{b}_{\mathbf{1}}^{\dagger}\hat{b}_{\nu}\hat{b}_{\mu} + V_{\nu 1\mu 1}\hat{b}_{\nu}^{\dagger}\hat{b}_{\mathbf{1}}\hat{f}_{\mu}^{\dagger}\hat{f}_{\mathbf{1}} + V_{\mathbf{1}\nu 1\mu}\hat{b}_{\mathbf{1}}^{\dagger}\hat{b}_{\nu}\hat{f}_{\mathbf{1}}^{\dagger}\hat{f}_{\mu}\big). \tag{B3}$$

Only local contributions are taken into account and thus the spatial index $\mathbf{j}$ is omitted for the moment. The intraband contributions are defined as the band energy

$$\Delta_{\nu}^{x} = \int d^3r\, \bar{w}_{\nu}^{x}(\mathbf{r})\left(-\frac{\hbar^2}{2m_x}\Delta + V^{x}(\mathbf{r})\right) w_{\nu}^{x}(\mathbf{r}) \tag{B4}$$

and the intraband nearest-neighbor hopping for bosons,

$$J_{\nu} = \int d^3r\, \bar{w}_{\nu}^{b}(\mathbf{r}-\hat{\mathbf{e}})\left(-\frac{\hbar^2}{2m_b}\Delta + V^{b}(\mathbf{r})\right) w_{\nu}^{b}(\mathbf{r}) \tag{B5}$$

and, correspondingly, for fermions $\widetilde{J}_{\nu}$.

APPENDIX C: FULL EFFECTIVE FIRST-BAND BFHM

Under the assumptions made in the main text (i.e., only local contributions, nearest-neighbor hopping, etc.), the final form of the effective Hamiltonian is found from Eqs. (A5) together with the interband couplings from Eqs. (B1)–(B3) in the Markov approximation. This yields

$$\begin{aligned}\hat{H}_{\mathbf{1}}^{\mathrm{eff}} = \hat{H}_{\mathbf{1}} &+ \sum_{\nu\neq\mathbf{1}}\sum_{\mathbf{jd}}\Bigg(\frac{(V_{\nu 1\nu 1})^2\mathcal{I}_{bf,\nu\nu}^{\mathbf{d}}}{4}\,\hat{b}_{\mathbf{j}+\mathbf{d}}^{\dagger}\hat{f}_{\mathbf{j}+\mathbf{d}}^{\dagger}\hat{f}_{\mathbf{j}}\hat{b}_{\mathbf{j}} + (U_{\nu 111})^2\mathcal{I}_{b,\nu}^{\mathbf{d}}\hat{b}_{\mathbf{j}+\mathbf{d}}^{\dagger}\hat{n}_{\mathbf{j}+\mathbf{d}}\,\hat{n}_{\mathbf{j}}\hat{b}_{\mathbf{j}} + \frac{U_{\nu 111}V_{\nu 111}\mathcal{I}_{b,\nu}^{\mathbf{d}}}{2}\,\hat{m}_{\mathbf{j}+\mathbf{d}}\hat{b}_{\mathbf{j}+\mathbf{d}}^{\dagger}\hat{n}_{\mathbf{j}}\hat{b}_{\mathbf{j}}\\ &+ \frac{V_{\nu 111}U_{\nu 111}\mathcal{I}_{b,\nu}^{\mathbf{d}}}{2}\,\hat{b}_{\mathbf{j}+\mathbf{d}}^{\dagger}\hat{n}_{\mathbf{j}+\mathbf{d}}\hat{m}_{\mathbf{j}}\hat{b}_{\mathbf{j}} + \frac{(V_{\nu 111})^2\mathcal{I}_{b,\nu}^{\mathbf{d}}}{4}\,\hat{m}_{\mathbf{j}+\mathbf{d}}\hat{b}_{\mathbf{j}+\mathbf{d}}^{\dagger}\hat{m}_{\mathbf{j}}\hat{b}_{\mathbf{j}} + \frac{(V_{11\nu 1})^2\mathcal{I}_{f,\nu}^{\mathbf{d}}}{4}\,\hat{n}_{\mathbf{j}+\mathbf{d}}\hat{f}_{\mathbf{j}+\mathbf{d}}^{\dagger}\hat{n}_{\mathbf{j}}\hat{f}_{\mathbf{j}}\Bigg)\\ &+ \sum_{\nu,\mu\neq\mathbf{1}}\sum_{\mathbf{jd}}\Bigg(\frac{(U_{\nu\mu 11})^2}{4}\,\mathcal{I}_{bb,\nu\mu}^{\mathbf{d}}(\hat{b}_{\mathbf{j}+\mathbf{d}}^{\dagger})^2\hat{b}_{\mathbf{j}}^2 + \frac{(V_{\nu 1\mu 1})^2}{4}\,\mathcal{I}_{bf,\nu\mu}^{\mathbf{d}}\hat{b}_{\mathbf{j}+\mathbf{d}}^{\dagger}\hat{f}_{\mathbf{j}+\mathbf{d}}^{\dagger}\hat{b}_{\mathbf{j}}\hat{f}_{\mathbf{j}}\Bigg).\end{aligned} \tag{C1}$$

In the Hamiltonian, the time integrals over the bosonic and fermionic correlators are defined as

$$\mathcal{I}_{b,\nu}^{\mathbf{d}} = -\frac{i}{\hbar}\int_0^{\infty} dT\,\langle\hat{b}_{\nu,\mathbf{j}+\mathbf{d}}(\tau+T)\hat{b}_{\nu,\mathbf{j}}^{\dagger}(\tau)\rangle, \tag{C2}$$

$$\mathcal{I}_{bf,\nu\mu}^{\mathbf{d}} = -\frac{i}{\hbar}\int_0^{\infty} dT\,\langle\hat{b}_{\nu,\mathbf{j}+\mathbf{d}}(\tau+T)\hat{b}_{\nu,\mathbf{j}}^{\dagger}(\tau)\rangle \times\langle\hat{f}_{\mu,\mathbf{j}+\mathbf{d}}(\tau+T)\hat{f}_{\mu,\mathbf{j}}^{\dagger}(\tau)\rangle, \tag{C3}$$

and, correspondingly, $\mathcal{I}_{f,\nu}^{\mathbf{d}}$ and $\mathcal{I}_{bb,\nu\mu}^{\mathbf{d}}$. The two-point correlation functions of bosons and fermions in the $\boldsymbol{\nu}$th band read

$$\langle\hat{b}_{\nu,\mathbf{j}+\mathbf{d}}(\tau+T)\hat{b}_{\nu,\mathbf{j}}^{\dagger}(\tau)\rangle_{\nu} = \frac{1}{L^3}\sum_{\mathbf{k}} e^{-2\pi i(\mathbf{k}\cdot\mathbf{d}/L^3)}e^{(i/\hbar)T\epsilon_{\mathbf{k}}^{b,\nu}}, \tag{C4}$$

$$\langle\hat{f}_{\nu,\mathbf{j}+\mathbf{d}}(\tau+T)\hat{f}_{\nu,\mathbf{j}}^{\dagger}(\tau)\rangle_{\nu} = \frac{1}{L^3}\sum_{\mathbf{k}} e^{-2\pi i(\mathbf{k}\cdot\mathbf{d}/L^3)}e^{(i/\hbar)T\epsilon_{\mathbf{k}}^{f,\nu}}. \tag{C5}$$

Carrying out the time integration in the thermodynamic limit, which is obtained for $L\to\infty$ by setting $\xi = \frac{\mathbf{k}}{L}$ and changing $\frac{1}{L^3}\sum_{\mathbf{k}}$ to $\iiint d^3\xi$, yields

$$\mathcal{I}_{x,\nu}^{\mathbf{d}} = \frac{1}{(2\pi)^3}\iiint d^3\xi\,\frac{e^{-i\xi\cdot\mathbf{d}}}{\epsilon^{x,\nu}(\xi)}, \tag{C6}$$

$$\mathcal{I}_{bx,\nu\mu}^{\mathbf{d}} = \frac{1+\delta_{\nu\mu}\delta_{bx}}{(2\pi)^6}\int\cdots\int d^3\xi\; d^3\xi'\,\frac{e^{-i\xi\cdot\mathbf{d}}e^{-i\xi'\cdot\mathbf{d}}}{\epsilon^{b,\nu}(\xi)+\epsilon^{x,\mu}(\xi')}. \tag{C7}$$

Here

$$\epsilon^{b,\nu}(\xi) = \sum_{\alpha=x,y,z} 2J_{\nu_\alpha}\cos(\xi_\alpha) + \Delta_{\nu_\alpha}^{b}, \tag{C8}$$

$$\epsilon^{f,\nu}(\xi) = \sum_{\alpha=x,y,z} 2\widetilde{J}_{\nu_\alpha}\cos(\xi_\alpha) + \Delta_{\nu_\alpha}^{f} \tag{C9}$$

is the energy of a boson and a fermion, respectively, in the higher band and x distinguishes between bosons ($x = b$) and fermions ($x = f$).

APPENDIX D: DEFINITION OF CONSTANTS IN THE HAMILTONIAN [EQ. (17)]

As used in the Hamiltonian of Eq. (17), the full expressions of the different parameters are the density-mediated fermionic or bosonic hopping,

$$\begin{aligned} &J[\hat{n}_{\mathbf{j}},\hat{n}_{\mathbf{j}+\hat{\mathbf{e}}},\hat{m}_{\mathbf{j}},\hat{m}_{\mathbf{j}+\hat{\mathbf{e}}}] \\ &\quad = J - J^b_{\mathrm{nl}}(\hat{n}_{\mathbf{j}+\hat{\mathbf{e}}} + \hat{n}_{\mathbf{j}}) - \frac{J^f_{\mathrm{nl}}}{2}\,(\hat{m}_{\mathbf{j}+\hat{\mathbf{e}}} + \hat{m}_{\mathbf{j}}) \\ &\qquad - \sum_{\boldsymbol{\nu}\neq\mathbf{1}} \mathcal{I}^{\hat{\mathbf{e}}}_{b,\boldsymbol{\nu}} \left\{ (U_{\boldsymbol{\nu}\mathbf{111}})^2\, \hat{n}_{\mathbf{j}+\hat{\mathbf{e}}}\hat{n}_{\mathbf{j}} + \frac{U_{\boldsymbol{\nu}\mathbf{111}}V_{\boldsymbol{\nu}\mathbf{111}}}{2}\, \hat{m}_{\mathbf{j}+\hat{\mathbf{e}}}\hat{n}_{\mathbf{j}} \right. \\ &\qquad \left. + \frac{V_{\boldsymbol{\nu}\mathbf{111}}U_{\boldsymbol{\nu}\mathbf{111}}}{2}\, \hat{n}_{\mathbf{j}+\hat{\mathbf{e}}}\hat{m}_{\mathbf{j}} + \frac{(V_{\boldsymbol{\nu}\mathbf{111}})^2}{4}\, \hat{m}_{\mathbf{j}+\hat{\mathbf{e}}}\hat{m}_{\mathbf{j}} \right\}, \end{aligned} \tag{D1}$$

$$\widetilde{J}[\hat{n}_{\mathbf{j}},\hat{n}_{\mathbf{j}+\hat{\mathbf{e}}}] = \widetilde{J} - \frac{\widetilde{J}_{\mathrm{nl}}}{2}\,(\hat{n}_{\mathbf{j}+\hat{\mathbf{e}}} + \hat{n}_{\mathbf{j}}) - \sum_{\boldsymbol{\nu}\neq\mathbf{1}} \frac{(V_{\mathbf{11}\boldsymbol{\nu}\mathbf{1}})^2\, \mathcal{I}^{\hat{\mathbf{e}}}_{f,\boldsymbol{\nu}}}{4}\, \hat{n}_{\mathbf{j}+\hat{\mathbf{e}}}n_{\mathbf{j}}; \tag{D2}$$

the pair tunneling amplitude,

$$\begin{aligned} J^{(2)} &= \frac{U^{\mathbf{j}+\hat{\mathbf{e}},\mathbf{j},\mathbf{j}+\hat{\mathbf{e}},\mathbf{j}}_{\mathbf{1111}}}{2} + \sum_{\boldsymbol{\nu}\neq\mathbf{1}} \frac{(U_{\boldsymbol{\nu}\boldsymbol{\nu}\mathbf{11}})^2 \mathcal{I}^{\hat{\mathbf{e}}}_{bb,\boldsymbol{\nu}\boldsymbol{\nu}}}{2} \\ &\quad + \sum_{\substack{\boldsymbol{\nu},\boldsymbol{\mu}\neq\mathbf{1} \\ \boldsymbol{\nu}\neq\boldsymbol{\mu}}} \frac{(U_{\boldsymbol{\nu}\boldsymbol{\mu}\mathbf{11}})^2 \mathcal{I}^{\hat{\mathbf{e}}}_{bb,\boldsymbol{\nu}\boldsymbol{\mu}}}{4}, \end{aligned} \tag{D3}$$

$$\begin{aligned} \widetilde{J}^{(2)} &= \frac{V^{\mathbf{j}+\hat{\mathbf{e}},\mathbf{j},\mathbf{j}+\hat{\mathbf{e}},\mathbf{j}}_{\mathbf{1111}}}{2} + \sum_{\boldsymbol{\nu}\neq\mathbf{1}} \frac{(V_{\boldsymbol{\nu}\mathbf{1}\boldsymbol{\nu}\mathbf{1}})^2 \mathcal{I}^{\hat{\mathbf{e}}}_{bf,\boldsymbol{\nu}\boldsymbol{\nu}}}{4} \\ &\quad + \sum_{\substack{\boldsymbol{\nu},\boldsymbol{\mu}\neq\mathbf{1} \\ \boldsymbol{\nu}\neq\boldsymbol{\mu}}} \frac{(V_{\boldsymbol{\nu}\mathbf{1}\boldsymbol{\mu}\mathbf{1}})^2}{4}\, \mathcal{I}^{\hat{\mathbf{e}}}_{bf,\boldsymbol{\nu}\boldsymbol{\mu}}; \end{aligned} \tag{D4}$$

the renormalized two-particle interactions,

$$U_2 = U + \sum_{\boldsymbol{\nu}\neq\mathbf{1}} (U_{\boldsymbol{\nu}\mathbf{111}})^2 \mathcal{I}^{\mathbf{0}}_{b,\boldsymbol{\nu}} + \sum_{\boldsymbol{\nu},\boldsymbol{\mu}\neq\mathbf{1}} \frac{1}{4} (U_{\boldsymbol{\nu}\boldsymbol{\mu}\mathbf{11}})^2 \mathcal{I}^{\mathbf{0}}_{bb,\boldsymbol{\nu}\boldsymbol{\mu}}, \tag{D5}$$

$$\begin{aligned} V_2 &= V + \sum_{\boldsymbol{\nu}\neq\mathbf{1}} \frac{(V_{\boldsymbol{\nu}\mathbf{1}\boldsymbol{\nu}\mathbf{1}})^2 \mathcal{I}^{\mathbf{0}}_{bf,\boldsymbol{\nu}\boldsymbol{\nu}}}{2} \\ &\quad + \sum_{\boldsymbol{\nu}\neq\mathbf{1}} \left(\frac{(V_{\boldsymbol{\nu}\mathbf{111}})^2 \mathcal{I}^{\mathbf{0}}_{b,\boldsymbol{\nu}}}{2} + \frac{(V_{\mathbf{1}1\boldsymbol{\nu}\mathbf{1}})^2 \mathcal{I}^{\mathbf{0}}_{f,\boldsymbol{\nu}}}{2} \right) \\ &\quad + \sum_{\substack{\boldsymbol{\nu},\boldsymbol{\mu}\neq\mathbf{1} \\ \boldsymbol{\nu}\neq\boldsymbol{\mu}}} \frac{(V_{\boldsymbol{\nu}\mathbf{1}\boldsymbol{\mu}\mathbf{1}})^2}{2}\, \mathcal{I}^{\mathbf{0}}_{bf,\boldsymbol{\nu}\boldsymbol{\mu}}; \end{aligned} \tag{D6}$$

and the three-body interactions,

$$U_3 = 6 \sum_{\boldsymbol{\nu}\neq\mathbf{1}} (U_{\boldsymbol{\nu}\mathbf{111}})^2 \mathcal{I}^{\mathbf{0}}_{b,\boldsymbol{\nu}}, \tag{D7}$$

$$V_3 = \sum_{\boldsymbol{\nu}\neq\mathbf{1}} \left(U_{\boldsymbol{\nu}\mathbf{111}} V_{\boldsymbol{\nu}\mathbf{111}} \mathcal{I}^{\mathbf{0}}_{b,\boldsymbol{\nu}} + \frac{(V_{\mathbf{11}\boldsymbol{\nu}\mathbf{1}})^2 \mathcal{I}^{\mathbf{0}}_{f,\boldsymbol{\nu}}}{4} \right). \tag{D8}$$

APPENDIX E: LATTICE EFFECTS

The lattice potentials for bosons and fermions are both created by the same laser field and the only externally controllable parameter is the intensity of this lattice laser. In order to see how the parameters of the effective lattice model, such as tunneling rates and interaction constants, depend on this laser intensity one needs to take into account that there is always a fixed ratio $\widetilde{f}$ between the bosonic and fermonic potential depths for given atomic species and transitions. To determine $\widetilde{f}$ we note that the optical lattice is generated by an off-resonant standing laser field. The potential itself results from the ac Stark shift. As shown in Ref. [36], it is given by

$$V_{\mathrm{pot}}(\mathbf{r}) = \frac{3\pi c^2}{2} \left(\frac{\Gamma_{D_1}}{\omega^3_{0,D_1}\Delta_{D_1}} + \frac{2\Gamma_{D_2}}{\omega^3_{0,D_2}\Delta_{D_2}} \right) I(\mathbf{r}) \tag{E1}$$

in the rotating-wave approximation for a typical alkali-metal D-line doublet, where each line contributes independently if the laser is sufficiently far detuned from the atomic transitions. The important parameters are the decay rates $\Gamma_{D_{1,2}}$ of the excited states; the detunings $\Delta_{D_{1,2}} = \omega_{\mathrm{laser}} - \omega_{0,D_{1,2}}$ of the laser frequency ω_{laser} from the atomic transition frequencies, $\omega_{0,D_{1,2}}$; and the laser intensity $I(\mathbf{r}) = I_0 \sin^2(\mathbf{k}\cdot\mathbf{r})$.

Conveniently, all energies in the system are normalized to the recoil energy of the bosonic species given by $E^b_{\mathrm{rec}} = \frac{\hbar^2 k^2}{2m_b}$. The wave number $\mathbf{k}$ depends on the chosen optical lattice. The (normalized) lattice potential for the bosons thus reads $V^b_{\mathrm{lat}}(\mathbf{r}) = \eta_b \sin^2(\mathbf{k}\cdot\mathbf{r})$. It is useful to rewrite the optical lattice potential for the fermionic atoms with respect to the bosonic optical lattice as $V^f_{\mathrm{lat}}(\mathbf{r}) = \eta_f \sin^2(\mathbf{k}\cdot\mathbf{r})$, where $\eta_f = \widetilde{f}\eta_b$. From Eq. (E1) we find

$$\widetilde{f} = \frac{\dfrac{\Gamma^f_{D_1}}{\left(\omega^f_{0,D_1}\right)^3\Delta^f_{D_1}} + \dfrac{2\Gamma^f_{D_2}}{\left(\omega^f_{0,D_2}\right)^3\Delta^f_{D_2}}}{\dfrac{\Gamma^b_{D_1}}{\left(\omega^b_{0,D_1}\right)^3\Delta^b_{D_1}} + \dfrac{2\Gamma^b_{D_2}}{\left(\omega^b_{0,D_2}\right)^3\Delta^b_{D_2}}}. \tag{E2}$$

At this point, we specify the experimental system. In the preceding discussion we analyzed the experiment reported in Ref. [16] and use the parameters given there. A mixture of bosonic ^{87}Rb and fermionic ^{40}K is cooled and put into an optical lattice with $\sigma_L = 755$ nm. For rubidium and potassium, the transition wavelengths and decay rates are given by

$$\begin{aligned} \sigma^{\mathrm{K}}_{D_1} &= 766.5\ \mathrm{nm}, \quad \sigma^{\mathrm{Rb}}_{D_1} = 795.0\ \mathrm{nm}; \\ \Gamma^{\mathrm{K}}_{D_1} &= 38.7 \times 10^6\ \mathrm{Hz}, \quad \Gamma^{\mathrm{Rb}}_{D_1} = 36.1 \times 10^6\ \mathrm{Hz}; \\ \sigma^{\mathrm{K}}_{D_2} &= 769.9\ \mathrm{nm}, \quad \sigma^{\mathrm{Rb}}_{D_2} = 780.2\ \mathrm{nm}; \\ \Gamma^{\mathrm{K}}_{D_2} &= 38.2 \times 10^6\ \mathrm{Hz}, \quad \Gamma^{\mathrm{Rb}}_{D_2} = 38.1 \times 10^6\ \mathrm{Hz} \end{aligned} \tag{E3}$$

By using these values, $\widetilde{f}$ in Eq. (E2) evaluates to $\widetilde{f} = 2.040\,43$, which means that the fermionic lattice potential, in terms of the bosonic recoil energy, is twice as deep as the bosonic one. However, for the calculation of the Wannier functions of bosons and fermions one has to take into account also the different masses of the particles. By expressing the Schrödinger equation for the single-particle fermionic wave function $\Phi_f(\mathbf{r})$ in terms of the bosonic quantities η_b and m_b, one finds

$$\left(-\frac{\hbar^2}{2m_b}\Delta + \frac{m_f}{m_b}\widetilde{f}\eta_b \sin^2(\mathbf{k}\cdot\mathbf{r})\right)\Phi_f(\mathbf{r}) = \frac{m_f}{m_b}E\Phi_f(\mathbf{r}). \tag{E4}$$

One recognizes that the difference between the fermionic and bosonic Wannier functions is determined only by the factor $\frac{m_f}{m_b}\widetilde{f}$. Since for the experiment in Ref. [16]

$$\frac{E^f_{\mathrm{rec}}}{E^b_{\mathrm{rec}}} = \frac{m_b}{m_f} = 2.175, \tag{E5}$$

the factor $\widetilde{f}$ is almost offset, $\frac{m_f}{m_b}\widetilde{f} = 0.93$. Thus the bosonic and fermionic Wannier functions are, to a good approximation, identical to a maximal overlap. Nevertheless, Fig. 3 also display results including a mismatch of the bosonic and fermionic Wannier functions, depicted by the gray-shaded regions. The upper (lower) boundary on the attractive side and the lower (upper) boundary on the repulsive side correspond to the results for a mismatch of $\frac{m_f}{m_b}\widetilde{f} = 0.7$ ($\frac{m_f}{m_b}\widetilde{f} = 1.3$), indicating the importance of a good control of the mismatch in the precise determination of the transition shift.

[1] D. Jaksch, C. Bruder, J. I. Cirac, C. W. Gardiner, and P. Zoller, Phys. Rev. Lett. **81**, 3108 (1998).
[2] R. Jördens, N. Strohmaier, K. Günter, H. Moritz, and T. Esslinger, Nature (London) **455**, 204 (2008).
[3] U. Schneider, L. Hackermüller, S. Will, T. Best, I. Bloch, T. A. Costi, R. W. Helmes, D. Rasch, and A. Rosch, Science **322**, 1520 (2008).
[4] L.-M. Duan, E. Demler, and M. D. Lukin, Phys. Rev. Lett. **91**, 090402 (2003).
[5] A. B. Kuklov and B. V. Svistunov, Phys. Rev. Lett. **90**, 100401 (2003).
[6] T. Barthel, C. Kasztelan, I. P. McCulloch, and U. Schollwöck, Phys. Rev. A **79**, 053627 (2009).
[7] A. Albus, F. Illuminati, and J. Eisert, Phys. Rev. A **68**, 023606 (2003).
[8] S. Will, T. Best, U. Schneider, L. Hackermuller, D.-S. Luhmann, and I. Bloch, Nature (London) **465**, 197 (2010).
[9] P. R. Johnson, E. Tiesinga, J. V. Porto, and C. J. Williams, New J. Phys. **11**, 093022 (2009).
[10] K. Günter, T. Stoferle, H. Moritz, M. Kohl, and T. Esslinger, Phys. Rev. Lett. **96**, 180402 (2006).
[11] S. Ospelkaus, C. Ospelkaus, O. Wille, M. Succo, P. Ernst, K. Sengstock, and K. Bongs, Phys. Rev. Lett. **96**, 180403 (2006).
[12] A. Mering and M. Fleischhauer, Phys. Rev. A **77**, 023601 (2008).
[13] M. Cramer, S. Ospelkaus, C. Ospelkaus, K. Bongs, K. Sengstock, and J. Eisert, Phys. Rev. Lett. **100**, 140409 (2008).
[14] L. Pollet, C. Kollath, U. Schollwöck, and M. Troyer, Phys. Rev. A **77**, 023608 (2008).
[15] C. N. Varney, V. G. Rousseau, and R. T. Scalettar, Phys. Rev. A **77**, 041608 (2008).
[16] T. Best, S. Will, U. Schneider, L. Hackermüller, D. van Oosten, I. Bloch, and D.-S. Lühmann, Phys. Rev. Lett. **102**, 030408 (2009).
[17] D. S. Lühmann, K. Bongs, K. Sengstock, and D. Pfannkuche, Phys. Rev. Lett. **101**, 050402 (2008).
[18] S. Tewari, R. M. Lutchyn, and S. Das Sarma, Phys. Rev. B **80**, 054511 (2009).
[19] R. M. Lutchyn, S. Tewari, and S. Das Sarma, Phys. Rev. A **79**, 011606 (2009).
[20] A. Mering and M. Fleischhauer, Deutsche Physikalische Gesellschaft Frühjahrstagung, Report No. Q 38.3, 2009 (unpublished).
[21] W. Kohn, Phys. Rev. **115**, 809 (1959).
[22] G. Mazzarella, S. M. Giampaolo, and F. Illuminati, Phys. Rev. A **73**, 013625 (2006).
[23] L. Amico, G. Mazzarella, S. Pasini, and F. S. Cataliotti, New J. Phys. **12**, 013002 (2010).
[24] In the three-dimensional system odd means that the number of odd elements in the multi-index ν has to be odd.
[25] H. Carmichael, *An Open Systems Approach to Quantum Optics* (Springer-Verlag, Berlin, 1993).
[26] A. Isacsson and S. M. Girvin, Phys. Rev. A **72**, 053604 (2005).
[27] N. Teichmann, D. Hinrichs, M. Holthaus, and A. Eckardt, Phys. Rev. B **79**, 100503 (2009).
[28] F. E. A. dos Santos and A. Pelster, Phys. Rev. A **79**, 013614 (2009).
[29] B. Capogrosso-Sansone, N. V. Prokof'ev, and B. V. Svistunov, Phys. Rev. B **75**, 134302 (2007).
[30] M. Greiner, O. Mandel, T. Esslinger, T. W. Hänsch, and I. Bloch, Nature (London) **415**, 39 (2002).
[31] M. Cramer, e-print arXiv:1009.4737.
[32] M. Snoek, I. Titvinidze, I. Bloch, and W. Hofstetter, Phys. Rev. Lett. **106**, 155301 (2011).
[33] A. Mering and M. Fleischhauer, Phys. Rev. A **81**, 011603(R) (2010).
[34] D. J. Klein, J. Chem. Phys. **61**, 786 (1974).
[35] R. Kubo, J. Phys. Soc. Jpn. **17**, 1100 (1962).
[36] R. Grimm, M. Weidemuller, and Y. B. Ovchinnikov, in *Advances in Atomic, Molecular and Optical Physics*, edited by B. Bederson and H. Walther (Academic, New York, 2000), Vol. 42, p. 95.